Numerical Study on the Quantitative Error of the Korteweg–de Vries Equation for Modelling Random Waves on Large Scale in Shallow Water

Jinghua Wang[a], Q.W. Ma[a,*] Shiqiang Yan[a] and Hongde Qin[b]

[a] School of Mathematics, Computer Science and Engineering, City, University of London, Northampton Square, London, EC1V 0HB, UK

[b] College of Shipbuilding Engineering, Harbin Engineering University, No.145 Nantong Street, 150001 Harbin, China

Abstract

The Korteweg–de Vries (KdV) equation is often adopted to simulate phase-resolved random waves on large scale in shallow water. It shows that the KdV equation is computationally efficient and can give sufficiently accurate results, but it is not always suitable and the error by using it cannot be predicted. This paper attempts to give the quantitative formulas for estimating the error of the statistics when simulating random waves in shallow water by using it. The formulas are obtained by fitting the errors of the KdV equation in comparison with the fully nonlinear model using the same initial condition based on the Wallops spectrum with a wide range of parameters. This paper also demonstrates how the formulas would be used, e.g., to estimate the error of the results by using the KdV model, or to justify its suitability for modelling random waves on large scale in shallow water.

Keywords: KdV equation; Fully nonlinear model; Random ocean waves; Large scale simulation; Phase-resolved models

1   Introduction

Shallow water random waves play an important role in engineering practices, and it is now increasingly recognized that accurate numerical simulation of such waves with sufficient nonlinearities is very necessary. The random feature

* Corresponding author at: School of Mathematics, Computer Science and Engineering, City, University of London, Northampton Square, London, EC1V 0HB, UK

Email: q.ma@city.ac.uk (Qingwei Ma)

of ocean waves and the nonlinear effects render the simulations being very challenging, let alone it needs to be carried out on a large scale for a long duration [1].

Successful numerical studies on modeling the shallow water waves have been carried out. Some employed the phase-averaged models, such as SWAN, etc., which are very popular among the oceanographers [2-7]. However, in engineering practice, direct phase-resolved information is always desired, e.g., velocity and acceleration field, free surface elevation and slope, etc., which requires simulation with the phase-resolved models. Among them, numerical models based on the Navier-Stokes (NS) equation or coupled potential-NS model is computationally prohibitive for large scale simulations and such applications in literature are rare. In contrast, the potential model is much faster and can give quite accurate results, thus a brief review is given below.

One class of such models are the fully nonlinear potential methods, such as Boundary Element Method [8, 9], Finite Element Method [10, 11] and Quasi Arbitrary Lagrangian-Eulerian Finite Element Method [12, 13]. However, they are still computationally expensive, thus barely applied so far to model waves in a scale of hundred wave lengths and thousand wave periods. Another category of the fully nonlinear potential methods is based on or associated with the Fast Fourier Transform (FFT), e.g., FFT mixed method [14-16], Irrotational Green-Naghdi model [17], Higher-Order Spectral (HOS) method [18, 19], Spectral Continuation method [20], Spectral Boundary Integral method [21-24] and Enhanced Spectral Boundary Integral (ESBI) method [25]. This class of models is relatively faster but still needs significant amount of time. For an example, a 3D random sea simulation covering 42×42 peak wave lengths for 250 peak wave periods takes 10 CPU days on a 3 GHz-Xeon single processor PC by using the HOS method [26].

In order to be more efficient, simplified models are employed for modeling random waves. One group of the models is the second order wave models, but they could not describe the continuous spectral energy transfer between wave components as the amplitude of each wave component was independent of time, and thus they were only accurate when the wave steepness was quite small (i.e., when the energy transfer between wave components was insignificant) [27, 28]. Another group is the envelope-type equations, such as the Zakharov equation [29-31] and the nonlinear Schrödinger equations [29-33]. However, these equations are only suitable for finite and deep water [34], thus will not be further discussed as our focus is the waves in shallow water in this paper.

Another class of the simplified models are the shallow water equations, such as the original Korteweg–de Vries (KdV) equation [35], the Benjamin-Bona-Mahony (BBM) equation [36], the Kadomtsev-Petviashvili (KP) equation [37], coupled KdV equation [38], perturbed KdV equation [34, 39-41], and the Boussinesq equation [42-45]. In this

paper, we only focus on 2-dimensional slip flat bottom situations where waves only propagate to the main direction, thus the original KdV equation, the BBM equation and Boussinesq model may be suitable for this purpose. However, the BBM equation is not convenient for numerical simulation in time domain. Meanwhile, although applications of the higher order version of Boussinesq equation on simulating random waves on local scale are extensive [46-50], and is more accurate compared with the KdV equation, its computational efficiency is relatively slow, even slower than some fully nonlinear models, which will be shown later in this paper. Therefore, it will not be employed either.

The authors are aware that the KdV equation can be very efficient and acceptable in terms of accuracy for modelling random waves on a large-spatial and long-temporal scale. For example, the statistical analysis based on the direct simulations of random wave fields and associated spectrum evolution in shallow water using the KdV equation [51, 52] provided useful information for understanding the behaviour of shallow water random waves. Sergeeva, et al. [53] also employed the KdV equation to study the statistics of random waves on a variable depth seabed and found that the probability of rogue waves increases in the transition zone. Dutykh, et al. [54] developed a geometric numerical scheme and employed it for solving the KdV equation. This scheme has been shown great robustness over simulating random seas on large scale, and it is found the probability of the free surface can be well represented by the truncated Gram-Charlier distribution. Toffoli, et al. [55] adopted the weakly three-dimensional version of KdV model (the so-called Kadomtsev-Petviashvili equation) to simulate random waves in crossing sea states, which indicated that interactions between the crossing wave trains can generate steep and high-amplitude waves. Very recently, the KdV equation is adopted to study the spectrum evolution in shallow water on large-scale (128 peak wave lengths) by specifying different wave steepness and Ursell numbers, and demonstrated that the equation can give a good prediction on the wave spectrum after a long-time (1000 peak periods) evolution when the Ursell number and wave steepness are both large [56].

However, one should be aware that the KdV equation is accurate in limited conditions, as it has limited capacity in resolving the nonlinearities [57], e.g., it becomes less accurate when the nonlinear effects of the second and higher order harmonics are large [58]. Osborne, et al. [59] had discussed the applicability of the KdV equation and indicated that it may be applicable only when the product of water depth and wave number is less than 1.14. While, a direct comparison between the results from FEM and KdV model is made by Sriram, et al. [60, 61] for simulating the propagation of solitary waves, where it is shown that good agreement is achieved if the Ursell number is small, otherwise the difference between the free surface simulated by using the FEM and KdV model becomes larger when

the Ursell number increases. Later, it has been pointed out that the KdV equation failed to describe the spectrum evolution in the cases where Ursell number is large while wave steepness is small [56]. As discussed above, the KdV equation, on the one hand, has been shown to be very efficient and sufficiently accurate in some cases, but on the other hand, its results are poor in some other cases. It is desired that one can quantitatively estimate the error of the KdV model when it is employed to simulate random waves. However, according to the existing literatures, the way to predict the error of the KdV model is unavailable.

Therefore, the main purpose of this paper is to give the quantitative formulas for estimating the error of using KdV equation to model the random waves on large scale for long duration, such as 128 peak wave lengths and 1000 peak periods. Besides, discussions about how to use this formula are also presented.

2   Methodologies

In order to obtain the quantitative errors, the fully nonlinear method (ESBI) and the KdV model will be applied to simulate a large number of cases, where the initial conditions are defined by the Wallops spectrum with a wide range of wave parameters. For each of the cases, the errors of the KdV models are estimated by comparing the skewness of the free surface with these obtained by using the ESBI. After the errors of all cases are obtained, the formulas are formulated by using a data fitting technique.

All the numerical models have been documented in the publications cited above and so their formulations will be only briefed for completeness. For convenience, all the variables involved will be non-dimensionalised in a consistent way, e.g., the length variables multiplied by peak wave number k_0, and the time variables multiplied by peak circular frequency ω_0, where $\omega_0 = \sqrt{gk_0\tanh(k_0h')}$, g is the gravitational acceleration, h' the dimensional water depth. More specifically, all the dimensionless variables used in this paper are listed in Table 1.

Table 1 Dimensionless variables

η	Surface elevation multiplied by k_0
$\boldsymbol{X} = (X, Y)$	Horizontal space coordinate multiplied by k_0
h	Water depth multiplied by k_0
T	Time multiplied by ω_0
c	Wave phase speed, which equals to $\sqrt{gh'}$ for shallow water multiplied by k_0/ω_0
H or H_s	Characteristic wave height H' or significant wave height H'_s multiplied by k_0. They actually represent wave steepness.
k_j	Wave number of an individual component multiplied by k_0^{-1}

a_j	Wave amplitude of an individual component multiplied by k_0
ω_j	Wave circular frequency of an individual component multiplied by ω_0^{-1}
T_0	Peak period multiplied by ω_0
$\phi, \tilde{\phi}$	Velocity potential and that at free surface multiplied by $\sqrt{k_0^3/g}$
$\boldsymbol{K} = (\kappa, \zeta), K$	Wave number coordinate and its module multiplied by k_0^{-1}
Ω	Wave circular frequency coordinate multiplied by ω_0^{-1}

2.1 The KdV model

The original KdV equation is adopted in this study, which can be expressed as [35],

$$\frac{1}{c}\frac{\partial \eta}{\partial T} = -\left(1 + \frac{3\eta}{2h}\right)\frac{\partial \eta}{\partial X} - \frac{h^2}{6}\left(1 - \frac{W}{3}\right)\frac{\partial^3 \eta}{\partial X^3} + O(\varepsilon^2, \varepsilon\mu^2, \mu^4) \tag{1}$$

where W is the Weber number measuring the effects of surface tension and is taken as zero in this study due to its neglectable effects, $\varepsilon = H/h \ll 1$, $\mu = h \ll 1$ and $O(\varepsilon) \sim O(\mu^2)$. Eq. (1) has also been employed to study the formation of rogue waves in shallow water [62].

It should be noted that Eq.(1) can also be reformulated without accounting for the error order term as [52]

$$\frac{\partial \zeta}{\partial \tau} = -\zeta \frac{\partial \zeta}{\partial \xi} - \frac{1}{9U_r}\frac{\partial^3 \zeta}{\partial \xi^3} \tag{2}$$

after the following substitutions are made

$$\zeta = \frac{\eta}{H}, \ \xi = X - cT, \tau = \frac{3cHT}{2h} \tag{3}$$

and the Ursell number $U_r = \varepsilon/\mu^2 = H/h^3$. Eq.(2) implies that the solution of KdV equation only depends on the magnitude of U_r. However, if higher order terms are preserved in Eq. (1) during the derivation of the KdV equation, then the solution to the KdV equation will also depend on the magnitude of ε, which means that the error by using Eq. (2) depends on not only Ursell number U_r but also wave height to depth ratio ε. This will be further discussed to explore the error of the KdV equation in Section 3 and 4.

In order to solve the KdV equation numerically, Eq.(2) can be integrated by using the fourth order Runge-Kutta method [63]. For completeness of this paper, this technique is briefed as follows.

i) At time step τ_0, $\zeta(\xi, \tau = \tau_0)$ is given initially or obtained from previous time step, then gradient $\partial\zeta/\partial\xi$ and $\partial^3\zeta/\partial\xi^3$ can be estimated through FFT;

ii) Estimate the Runge-Kutta coefficients, i.e., $\partial\zeta/\partial\tau_k$, where k = 1, 2, 3 and 4;

iii) Update the rescaled free surface by using the formula $\zeta(\xi, \tau = \tau_0 + \Delta\tau) = \zeta(\xi, \tau = \tau_0) + (\partial\zeta/\partial\tau_1 + 2\partial\zeta/\partial\tau_2 + 2\partial\zeta/\partial\tau_3 + \partial\zeta/\partial\tau_4)\Delta\tau/6$;

iv) If it has reached the end of the simulation, quit the simulation, otherwise go to step i).

To validate the numerical code for regular waves, cnoidal waves are simulated and its analytical solution is used as the initial condition. The solution for the cnoidal wave based on KdV equation, i.e., Eq.(1), has been derived by Korteweg & de Vries [35], which is presented here without further details,

$$\eta = \frac{H}{\mathcal{M}}\left(1 - \mathcal{M} - \frac{E}{\mathcal{K}}\right) + Hcn^2\left(\frac{\mathcal{K}}{\pi}X\right) \qquad (4)$$

where cn is the Jacobi elliptic function, $\mathcal{M}$ is the modulus determined by U_r, and $\mathcal{K}$ and E are the complete elliptic integral of first kind and second kind, respectively. Each specified U_r corresponds to a unique solution with respect to Eq.(4).

During numerical simulation, the domain covers 1 cnoidal wave length and is resolved into 64 points. The simulation lasts for 1000 cnoidal wave periods and the wave profiles at the initial and the end of the simulation by using different U_r are displayed in Figure 1. It is understood that there should be no phase shift between the profiles at the beginning and the end of the simulation if the numerical scheme is accurate enough. By looking at the results in Figure 1, it is found that the profiles at the end of the simulation coincides with the initial one for each specific U_r, in which the maximum error is about 0.5%. Thus the numerical scheme used for solving Eq.(2) is quite accurate.
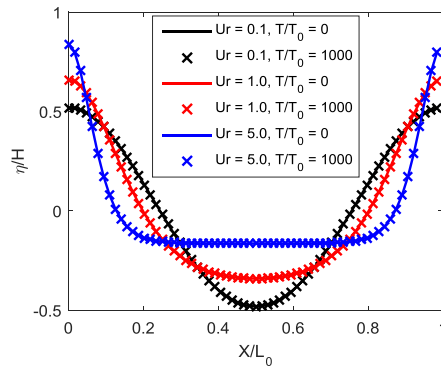

Figure 1. Free surface profiles for different Ursell number

Additionally, in order to validate our code for simulating random waves, another case reported in Pelinovsky & Sergeeva [52] is repeated here, where the Gaussian spectrum was employed as initial spectrum and evolution of spectrum was studied, where $U_r = H_s/h^3 = 0.95$ and $\sigma = 0.27$. The simulation is carried out to the 1000 peak periods in a domain covering 30 peak wave lengths, which is resolved into 1024 points. The spectrum at $T/T_0 = 0$,

194 and 970 by using the KdV model, in comparison with the results in Pelinovsky & Sergeeva [52] is shown in Figure 2. It implies that the results obtained by using the present code is consistent with that in Pelinovsky & Sergeeva [52], apart from minor differences which may be caused by using different random phases. Thus, the numerical code for solving the KdV model has been validated and will be adopted for the following study.
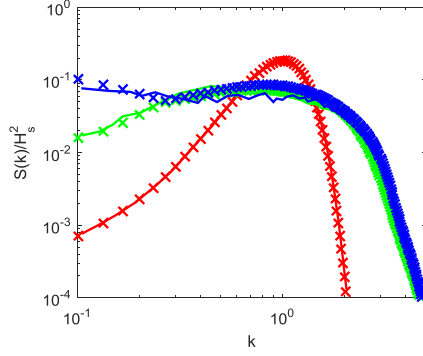

Figure 2. Spectra at different instant. '—': Pelinovsky & Sergeeva [52], 'x': present KdV code; Red is for $T/T_0 = 0$, green $T/T_0 = 194$ and blue $T/T_0 = 970$.

2.2 The ESBI model

The fully nonlinear model, referred as the Enhanced Spectral Boundary Integral (ESBI) method, has been recently developed by Wang & Ma [25], based on the formulations by Clamond & Grue [21], Grue [23], Fructus, et al. [22], Clamond, et al. [64] and Grue [24]. Details about the method will not be given here. However, the summary of main equations is presented for completeness.

The prognostic equation is given by

$$\frac{\partial \boldsymbol{M}}{\partial T} + A\boldsymbol{M} = \boldsymbol{N} \tag{5}$$

where

$$\boldsymbol{M} = \begin{pmatrix} KF\{\eta\} \\ K\Omega F\{\tilde{\phi}\} \end{pmatrix}, A = \begin{bmatrix} 0 & -\Omega \\ \Omega & 0 \end{bmatrix}, \boldsymbol{N} = \begin{pmatrix} K\big(F\{V\} - KtanhKhF\{\tilde{\phi}\}\big) \\ K\Omega F\left\{\frac{1}{2}\left[\frac{(V+\nabla\eta\cdot\nabla\tilde{\phi})^2}{1+|\nabla\eta|^2} - |\nabla\tilde{\phi}|^2\right]\right\} \end{pmatrix} \tag{6}$$

η and ϕ are the free surface elevation and velocity potential, respectively ($\tilde{\phi}$ is the value at free surface), $\nabla = \frac{\partial}{\partial X} = \frac{\partial}{\partial X}\boldsymbol{i} + \frac{\partial}{\partial Y}\boldsymbol{j}$ is the horizontal gradient operator, $V = \partial\phi/\partial n\sqrt{1 + |\nabla\eta|^2}$ is the vertical velocity, $\boldsymbol{K} = (\kappa, \lambda)$ is the wave

number, $K = |\boldsymbol{K}| = \sqrt{\kappa^2 + \lambda^2}$ and the circular frequency $\Omega = \sqrt{Ktanh(Kh)/\tanh(h)}$. All the aforementioned variables are nondimensionlized as shown in Table 1. The Fourier transform $F\{\ \}$ and the inverse transform $F^{-1}\{\ \}$ are defined as

$$\hat{\eta}(\boldsymbol{K}, T) = F\{\eta\} = \int_{-\infty}^{\infty} \eta(\boldsymbol{X}, T) e^{-i\boldsymbol{K}\cdot\boldsymbol{X}} d\boldsymbol{X} \tag{7}$$

$$\eta(\boldsymbol{X}, T) = F^{-1}\{\hat{\eta}\} = \frac{1}{4\pi^2} \int_{-\infty}^{\infty} \hat{\eta}(\boldsymbol{K}, T) e^{i\boldsymbol{K}\cdot\boldsymbol{X}} d\boldsymbol{K} \tag{8}$$

Fast Fourier Transform (FFT) is adopted to perform the Fourier and inverse transform numerically.

The solution to Eq.(5) is given as

$$\boldsymbol{M}(T) = e^{-A(T-T_0)}\left[\boldsymbol{M}(T_0) + \int_{T_0}^{T} e^{A(T-T_0)} \boldsymbol{N} dT\right] \tag{9}$$

where

$$e^{A\Delta T} = \begin{bmatrix} \cos\Omega\Delta T & -\sin\Omega\Delta T \\ \sin\Omega\Delta T & \cos\Omega\Delta T \end{bmatrix} \tag{10}$$

In addition, the solution to the vertical velocity can be derived with the help of the boundary integral equations, which is given as $V = V_1 + V_2 + V_3 + V_4$ involving the convolution and integration parts, and the formulations are presented in the appendix. The calculation of the convolutions is very fast owing to the algorithm of FFT whereas the integration parts are quite time consuming.

In the study by Wang & Ma [25], some numerical techniques have been proposed in order to improve the computational efficiency. Firstly, a new numerical de-singularity technique is introduced to evaluate the integration parts more efficiently. Secondly, they have reformulated the equations for $V_{3,s}$ in Eq. (A.5) and $V_{4,s}$ in Eq. (A.6) as

$$V_{3,s} = V_{3,C} + V_{3,I} = \underbrace{V_3^{(1)}}_{4th} + \underbrace{V_3^{(2)}}_{6th} + \underbrace{V_{3,I}}_{integration} \tag{11}$$

$$V_{4,s} = V_{4,C} + V_{4,I} = \underbrace{V_4^{(1)}}_{3rd} + \underbrace{V_4^{(2)}}_{5th} + \underbrace{V_4^{(3)}}_{7th} + \underbrace{V_{4,I}}_{integration} \tag{12}$$

During the simulation, the wave condition is examined. The integration parts are evaluated only when necessary; otherwise they are neglected. In such a way, computational time is saved without affecting the accuracy of numerical results. Thirdly, a new technique for anti-aliasing is developed for eliminating aliasing problems associated with convolutions. More details of the numerical scheme for the ESBI model and validation examples could be found in Wang & Ma [25] and will not be repeated here.

In order to validate and illustrate the efficiency of the ESBI, a comparison is made between the Boussinesq model [65] and the ESBI for simulating a focusing wave. In addition, the the fully nonlinear QALE-FEM model [12] is also used to demonstrate the accuracy of the ESBI model. The tank covers 32 peak wave lengths and is resolved into 128 points per peak wave length with a water depth $h = 0.5$. A focusing wave is generated at $X_f = 3L_0$ and $T_f = 25T_0$ based on Bretschneider spectrum [66] where $H_s = 0.0013$ $(U_r = H_s/h^3 \approx 0.01)$, and the simulation lasts for 35 peak periods. Good agreement is observed between the three models, as seen in Figure 3, where the error of the maximum surface elevation is about 4.3%. It indicates that the ESBI can be accurately used to simulate shallow water waves. In addition, the ESBI is about 11 times faster than the Boussinesq model, as the former costs 299s while the latter takes 3310s based on single-thread computation on a workstation with Intel® Xeon® CPU E5620@2.4GHz. Thus, the Boussinesq model will not be employed in this paper due to its relatively slower performance (more examples are reported in [67]).
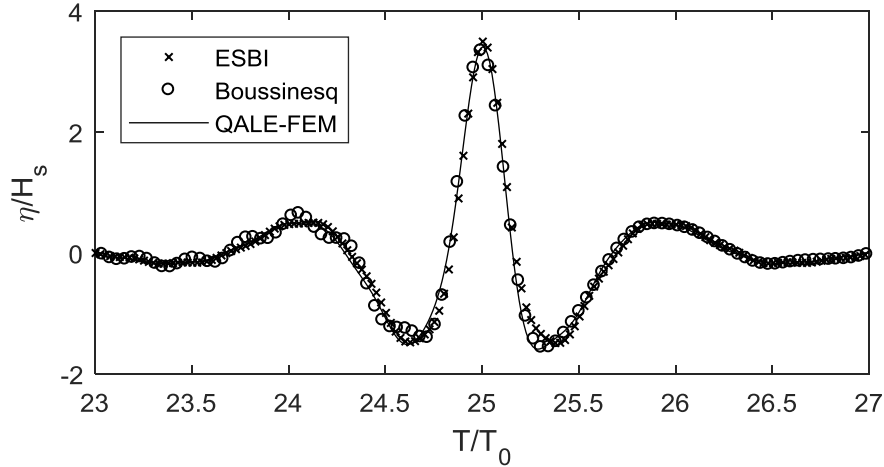

Figure 3. Time history at focusing location

3   Numerical simulations and results

The main purpose of this section is to identify the error of the results given by KdV model in Eq. (1), or equivalently, Eq. (4), by comparing its results with these from the fully nonlinear ESBI method in various different conditions in shallow water.

3.1 Computational parameters

In order to identify the error, the computational parameters need to be properly selected. The numerical simulation starts by specifying the initial values on the free surface, which are determined by using the Wallops spectrum and its parametric form [66] in terms of the wave number is used here, i.e.,

$$S(k) = \frac{\beta H_s^2}{k^m} exp\left(-\frac{m}{4k^4}\right) \tag{13}$$

where $\beta = 0.06238m^{(m-1)/4}/(4^{(m-5)/4}\Gamma[(m-1)/4])[1 + 0.7458(m+2)^{-1.057}]$. The bandwidth parameter $m = 3$ is used in this study, which is recommended for modelling shallow water waves [66].

Then the initial free surface is determined by using

$$\eta = \sum_{j=1}^{NJ} a_j \cos(k_j X + \varphi_j) \tag{14}$$

where $a_j = \sqrt{2S(k)\Delta k}$ is the amplitude, k_j is the wave number, φ_j is the random phase of jth component and NJ is the total number of the components. In this study, we choose $\Delta k = 1/128$ and cut-off wave number $k_{max} = 8$, which means that a total number of 1024 components are considered. It implies that the conclusion drawn by using Eq. (14) as the initial condition can also be applied to the cases where the random amplitude technique [69] is adopted as indicated in [70]. For a specific water depth, the wave train needs a considerable distance to relax towards a new equilibrium state as pointed out by Sergeeva, et al.[53], where they had simulated waves propagating on a scale of more than 26km~170 peak wave lengths. For the numerical studies, the computational domain is set as 128 peak wave lengths, which is more than 20 km if the peak wave period is 10 second or more. The domain is resolved into 8192 points for both the models, which is sufficient based on the pre-test. As pointed out by Pelinovsky & Sergeeva [52], the simulation duration of 1000 peak periods is sufficient to reach the equilibrium condition. Thus, the duration of the simulation lasts for 1000 peak periods, corresponding to a 3-hour sea state [56], which will be shown later to be sufficient for this study.

In order to estimate the error in the results of the KdV model, the skewness is employed [53]

$$\gamma = \frac{E[\eta^3]}{\sigma^3} \approx \frac{E[\eta^3]}{(H_s/4)^3} \tag{15}$$

where $E[*]$ denotes the expectation, σ is the standard deviation of free surface. The skewness is always used to measure the vertical asymmetry of the sea surface elevation, and larger value denotes stronger nonlinearity, e.g.,

sharper crest and flatter trough [62]. The relationship between the skewness and spectral bandwidth was established in [73], in which it is found that a variation of the spectral bandwidth is always accompanied by a variation of the skewness: the spectrum broadens until a new equilibrium is reached and the skewness becomes constant again. Based on that, the error is then estimated through

$$Err = \frac{1}{n_2 - n_1} \sum_{n=n_1+1}^{n_2} \Delta\gamma(T = nT_0) \tag{16}$$

where

$$\Delta\gamma(T = nT_0) = \frac{|E[\eta_1^3] - E[\eta_2^3]|}{(H_s/4)^3} \tag{17}$$

η_1 and η_2 are the free surface obtained by using the ESBI and KdV models, respectively, n_1 and n_2 are integers. To determine n_1 and n_2, two examples with $H_s = 0.08$ & $U_r = 3$ and $H_s = 0.04$ & $U_r = 2$ are simulated, and the corresponding results are shown in Figure 4. By looking at the results, it is found that the skewness reached quasi-stationary state [53] very soon (within 100 peak periods) in some cases, e.g., Figure 4(b), while it didn't become stabilized until $T/T_0 = 500$, e.g., Figure 4(a). It further confirms the importance of long-time simulation, and in this study, the skewness averaged within the last 500 peak periods will be employed to estimate the error, i.e., $n_1 = 500$ and $n_2 = 1000$.
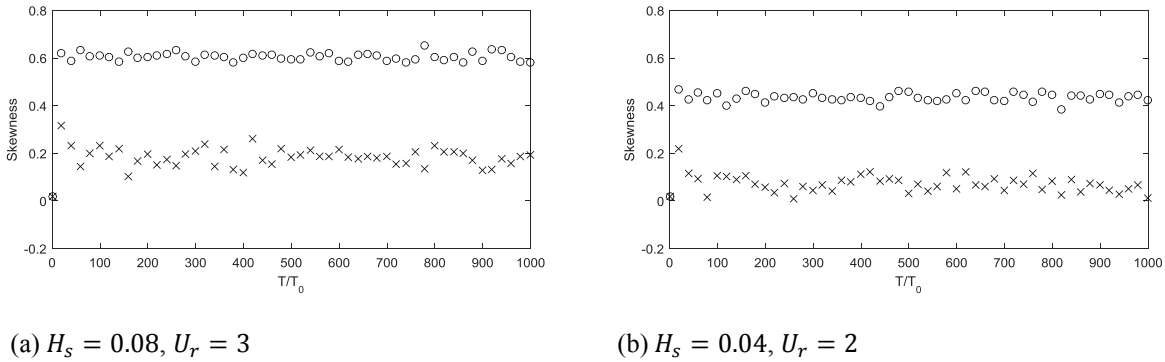

(a) $H_s = 0.08$, $U_r = 3$ (b) $H_s = 0.04$, $U_r = 2$

Figure 4. Skewness at different time instances based on ESBI ('x') and KdV ('o')

For the Wallops spectrum, the range of the nondimensional significant wave height H_s needs to be determined, which actually represents the steepness or nonlinearity of the initial free surface elevation as defined in Table 1. If it is very small, the waves can be well described by the linear model. Based on our pre-tests, 0.001 can be taken as the lower end of the range of H_s (i.e. its smallest value for the numerical study), and the linear model can very well predict the evolution of waves with $H_s < 0.001$.

The next question is how to determine the upper end of the range for H_s. It is understandable that with the increase of the wave steepness, the nonlinearities become stronger, so that the accuracy of the KdV model worsens and its error becomes larger. In practice, one just needs to quantify the error in a certain range, e.g., up to the error named as Err_{up}. The KdV model should be considered as unsuitable if its error exceeds Err_{up}, which is chosen as 10% in this paper. The upper end of H_s should be chosen to be the value, corresponding to which the error of the KdV model is smaller than Err_{up}. According to our later numerical tests, the upper end of H_s can be taken as 0.2, due to that numerical blow-up occurs for all cases when $H_s > 0.2$, which as indicated by Fructus, et al. [71], corresponds physically to the onset of wave breaking. Despite that the range of H_s is carefully selected, wave breaking is observed in some cases after a long-time propagation due to nonlinear effects. In that case, wave breaking is not suppressed through numerical techniques and the simulation is interrupted. And the authors choose to only consider cases of nonbreaking waves, which will be later shown to be sufficient to achieve the goal of this study, i.e., to quantify the error of the KdV model and to demonstrate its suitability. Whereas for the cases without observation of wave breaking, the probability of wave breaking is very unlikely if the duration is longer, since 1000 peak periods as the duration is already sufficiently long.

In addition, the range of the Ursell number should be chosen as well. According to Ursell [72], the KdV equation is derived by assuming $U_r \approx 1$, which implies that the KdV equation is not suitable when U_r is too large or too small. Thus we need to choose some values lower and higher than one, respectively. Based on our pre-tests, it is found that the error of the KdV model seems to converge to a stable value for a fixed H_s when U_r is sufficiently small. For example, the maximum deviation of the error between the cases $U_r = 0.1$ and $U_r = 0.01$ is 0.01. Therefore $U_r = 0.01$ is sufficiently small to quantify the error of the KdV model. It has been found during our numerical tests that the error quickly builds up and turns unacceptable when U_r increases. As aforementioned, the KdV model should be considered as unsuitable if its error is larger than Err_{up}. Similar with the way to choose the upper end of H_s, the maximum value for U_r considered in this study is 10. Based on the above discussions, the ranges of H_s and U_r chosen here are sufficient to quantify the error of the KdV model, and the values of each parameter are given in Table 2.

Table 2 Choice of parameters

H_s	0.001, 0.01, 0.02, 0.04, 0.06, 0.08, 0.1, 0.11, 0.12, 0.13, 0.15. 0.16, 0.18, 0.2
U_r	0.01, 0.1, 0.3, 0.4, 0.5, 0.55, 0.6, 0.65, 0.7, 0.75, 0.8, 0.9, 1, 1.2, 1.4, 1.6, 1.8, 2, 3, 5, 10

3.2   Error of the KdV model

The errors of the KdV model are then presented and discussed. In each case, both the models start with the same initial free surface determined by Eq.(14). Then Eq. (17) is used to calculate $\Delta\gamma$ at every peak period and the error is estimated by using Eq. (16). The values of the skewness by using both the methods are displayed in Figure 5, where some data points are missing due to the calculated wave breaking. As shown in the figure, the skewness calculated by using the ESBI model depends both on wave steepness and Ursell number, while that of the KdV model only depends on the Ursell number and is independent of wave steepness. Then by using the calculated skewness, the obtained numerical errors are shown in Figure 6, where the error larger than 0.1 is not displayed. As can be seen, for each fixed H_s, i.e., along the curve of Err in terms of U_r, there is a minimum point, denoted by (H_{s0}, U_{r0}). Connected all these points, one has a dash line on the $H_s - U_r$ plane as seen in the figure. This line can be regarded as the optimum points for the KdV model for simulating random seas, i.e., minimum errors are obtained. Based on that, the whole surface can be split into two parts: on the left, the error of the KdV model generally increases with the decrease of U_r, while it is opposite on the right side. It is understandable that the KdV model becomes less accurate when U_r is too small or too large, as pointed out earlier in this paper. In particular, the error becomes very large (more than 0.1) when $U_r > 1.6$.

To mathematically represent the calculated errors in Figure 6, we assume that the dash line can be fitted by $U_{r0} = \alpha H_{s0}^{\beta} + \delta$, while the errors on each side of the dash line can be fitted by $Err_i = a_i(H_s + b_iU_r + c_i)(U_r + d_i) + e_i$, where $\alpha, \beta, \delta, a_i, b_i, c_i, d_i$ and e_i are constants to be determined, i = 1 or 2 corresponding to the left or right part respectively. This function gives the best fitting results, which is selected through competing with other functions (details are omitted). The optimization is performed by using the toolbox (Optimization-fminsearch) in MATLAB. The details can be found in MATLAB help manual which will not be provided here for simplicity. Since the error larger than 0.1 may just indicate the KdV model is not suitable, only the data corresponding to $Err < 0.1$ are considered for fitting. After the constants are optimised, the mathematical expressions are given by

$$U_{r0} = 2.58 \times H_{s0}^{0.608} + 0.059 \tag{18a}$$

$$Err_1 = -0.127(H_s + 0.55U_r + 4.432)(U_r - 7.092) - 3.985, \quad U_r \leq U_{r0} \tag{18b}$$

$$Err_2 = -0.386(H_s - 0.146U_r - 0.209)(U_r + 1.24) - 0.15, \quad U_r > U_{r0} \tag{18c}$$

where $Err_i = 0$ (i=1 or 2) if its value is negative. The fitted curve by Eq. (18a) and the fitted surfaces by Eqs.(18b) and (18c) are shown in Figure 7 and Figure 8, respectively. Excellent consistency is observed between the calculated and fitted results. The maximum error between the calculated and fitted results in Figure 7 is only 2.4%. Meanwhile, the maximum deviations between the calculated and fitted errors in Figure 8 (a) and (b) are 0.013 and 0.036 respectively.

It is noted that Eqs.(18) are obtained by using the parameters in Table 2, thus it is understandable that they can only be applied within the range $0.001 \leq H_s \leq 0.2$ and $0.01 \leq U_r \leq 10$. However, taking all the facts into accounts and based on the discussions in this section, one may conclude that: (i) When $H_s < 0.001$, the linear model can be used without significant error; (ii) When $H_s > 0.2$, wave breaking likely occurs or the error is larger than 10% and the KdV model cannot be used; (iii) When $0.001 \leq H_s \leq 0.2$, the error of the KdV model is larger than 0.1 if $U_r > 1.6$, so that it cannot be employed; (iv) Since the error of the KdV model approximately equals to the case $U_r = 0.01$ if $U_r < 0.01$, one can estimate the error of the KdV model by using Eqs.(18) when $U_r \leq 1.6$: if the error is less than 0.1, one may accept this error by using the KdV model, while if the error is larger than 0.1, the KdV model may not be employed. More discussions about how to use Eqs.(18) will be provided in the following section.
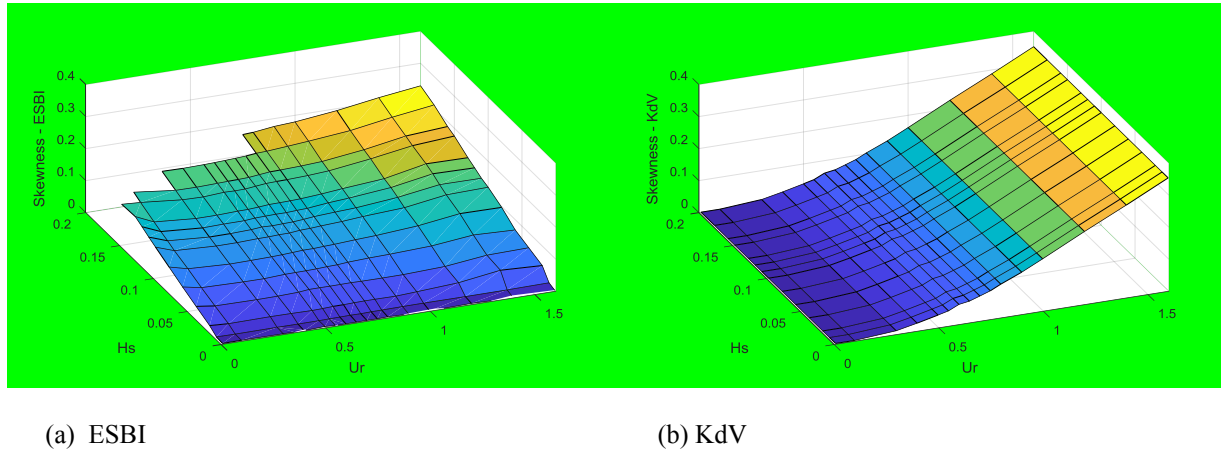

(a) ESBI

(b) KdV

Figure 5. Calculated skewness
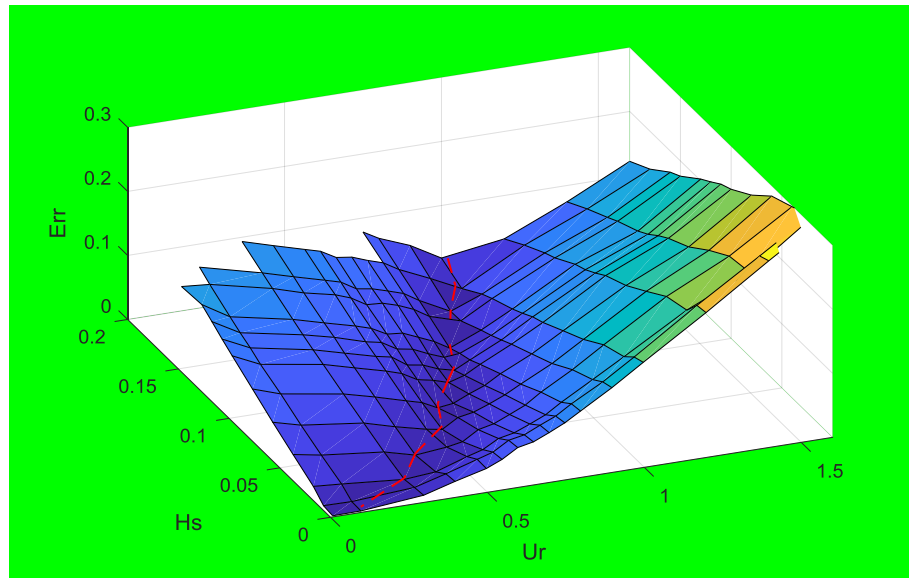
Figure 6. Error against H_s and U_r

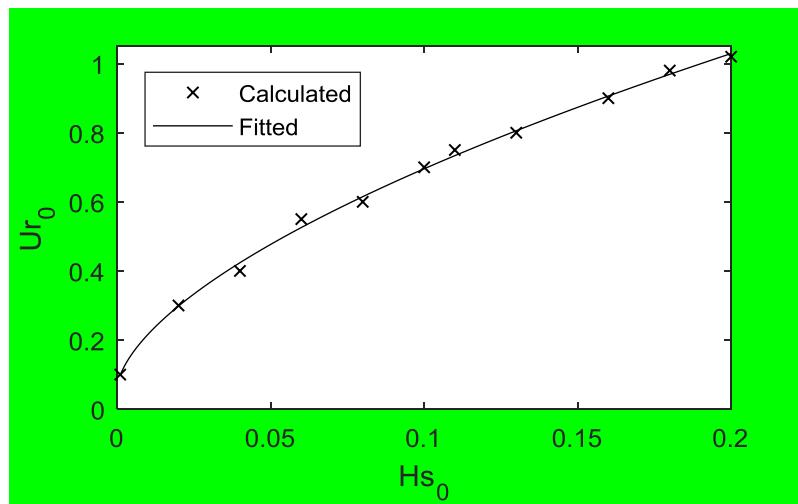Figure 7. Target and fitted U_{r0} and H_{s0}

<div align="center">(a)</div>
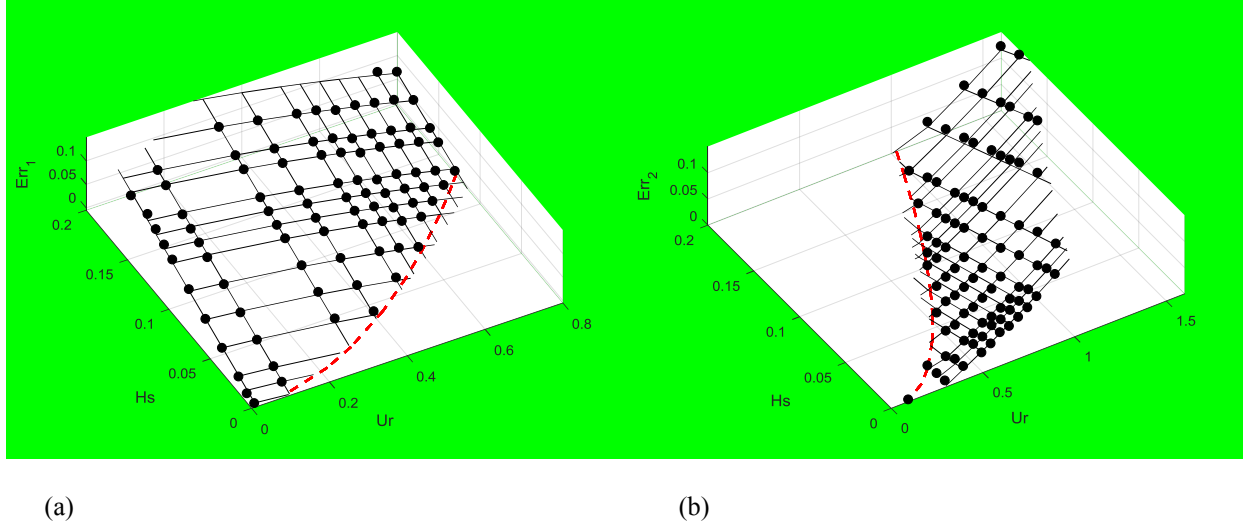<div align="center">(b)</div>

<div align="center">Figure 8. Calculated errors ' ● ' and fitted results '—'. Red dash line denotes U_{r0}-H_{s0}</div>

4   Discussion on the applications

Eqs.(18) obtained above may be employed for different purposes. Firstly, if the KdV equation is employed due to its advantage on the efficiency, such as a rough estimation of wave dynamics for conception design, one can use those equations to estimate the error of results obtained by using the KdV equation. To indicate the efficiency of the KdV model, the computational time is given here which is taken from a single case of $H_s = 0.15 \& U_r = 0.8$: the ESBI costs 4500s~1.25hour, meanwhile the KdV equation only needs 413s~6.8min to finish one run with single thread computing on Intel® Xeon CPU (E5-2630 v2@2.6GHz). Secondly, one may reformulate those equations to justify the suitability of the KdV model for simulating random waves in shallow water. Details and some examples are provided below.

4.1   Error estimation

To illustrate the effectiveness of Eqs.(18) for estimating the error, extra numerical tests are carried out for the cases with parameters listed in Table 3, which are in the range of Table 2 but are different from those used for Figure 6. In the table, the values of Err are obtained in the same way as for Figure 6, while the values of Err_i are predicted by using Eqs.(18). It is found that although the choices of the parameters differ from that in Figure 6, Eqs.(18) can still satisfactorily give accurate prediction of the error as long as $Err \leq 0.1$, even in some cases where $Err > 0.1$. The maximum deviation between the calculated and predicted errors in these cases is about 0.024, which is below the maxima obtained in section 3.

The errors given in Eqs.(18) are based on skewness of the free surface, the next question is what the probability density of the free surface or the spectrum looks like if the error in terms of the skewness is less than 0.1. To answer this question, some results of the probability density of the free surface and the corresponding spectra with respect to different levels of errors are displayed in Figure 9, where only $\eta/H_s \geq 0$ for probability density is shown for clarity. As can be seen in the figures, when the error is small, e.g., less than 0.05, the curve of the probability density obtained by using the KdV model looks very similar with that by using the ESBI model, so are the spectra, as shown in Figure 9 (a) and (b), respectively. While the difference between them becomes larger and larger when the error increases, and turns to be unacceptable when the error exceeds 0.1 as shown in Figure 9 (g) and (h).
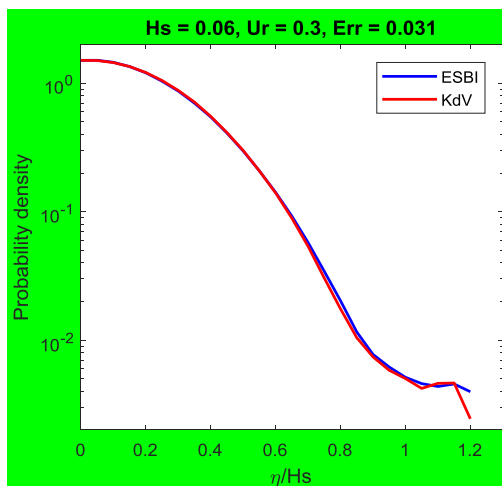
Table 3 Comparison between the numerical and predicted results

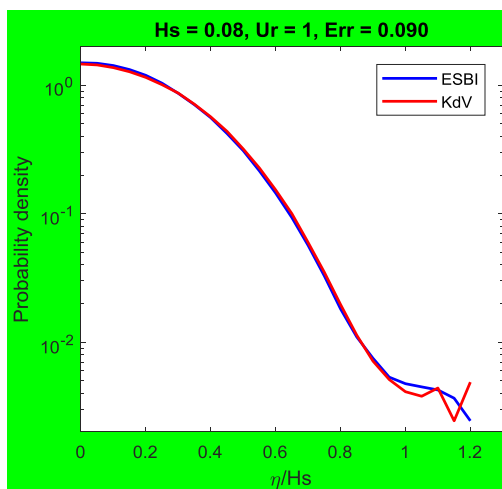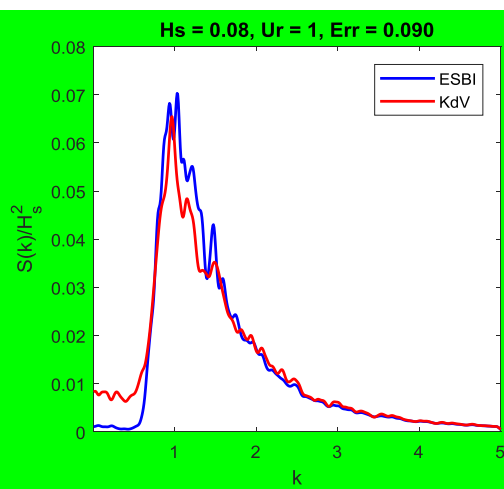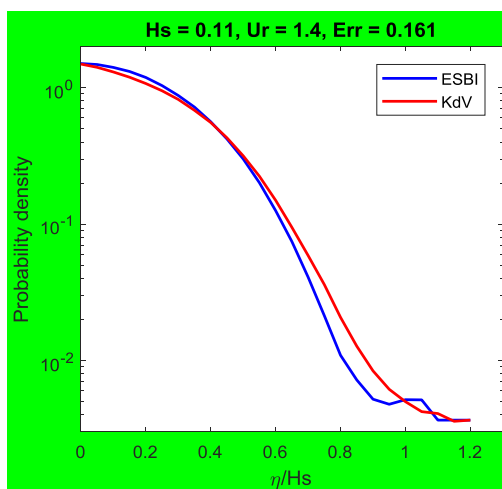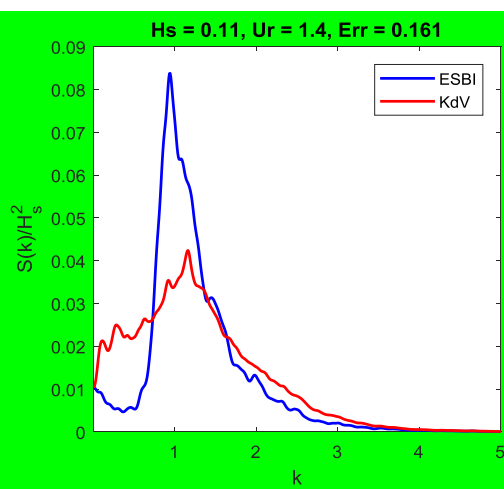|	$U_r = 1.1$		$U_r = 0.45$		$U_r = 0.2$		$U_r = 0.1$	
	Err	Err_i	Err	Err_i	Err	Err_i	Err	Err_i
$H_s = 0.005$	0.193	0.179	0.034	0.026	0.004	0.000	3E-4	4E-3
$H_s = 0.05$	0.159	0.139	0.007	0.000	0.026	0.034	0.032	0.043
$H_s = 0.09$	0.119	0.103	0.022	0.038	0.058	0.069	0.065	0.079
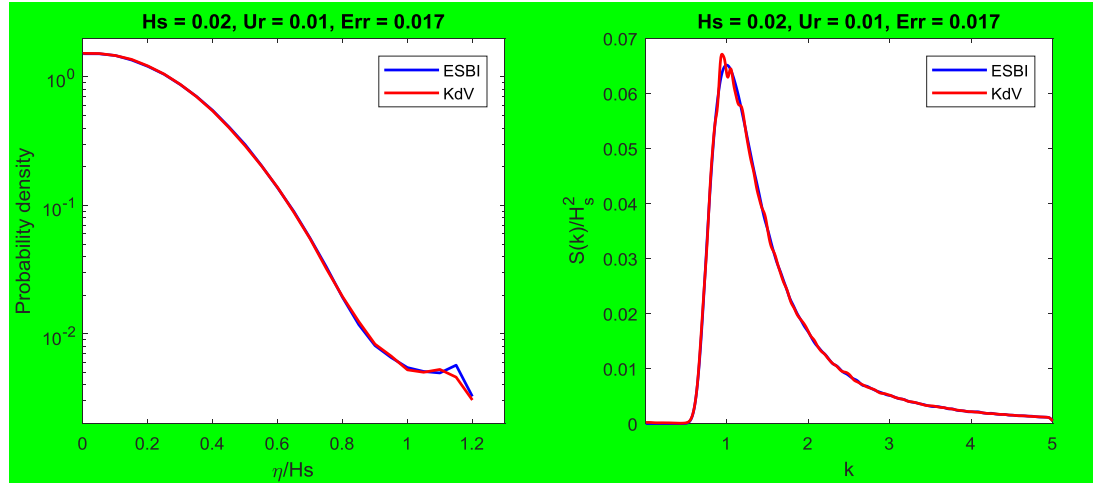
(a)

(b)

(c)
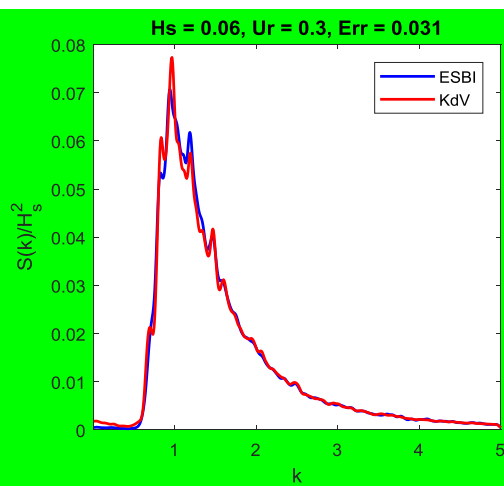
(d)

(e)

(f)

(g)

(h)

Figure 9. Probability density of free surface (a, c, e & g) and corresponding spectra (b, d, f & h)

In addition, the kurtosis is also an important factor that represents the probability of the extreme waves [62], and one may also ask if Eqs.(18) can be used to predict the error of kurtosis. To answer this question, the error of the kurtosis is estimated by using the formula

$$Err_\kappa = \frac{1}{n_2 - n_1} \sum_{n=n_1+1}^{n_2} \Delta\kappa(T = nT_0)$$ (19)

where

$$\Delta\kappa(T = nT_0) = \frac{\left|E[\eta_1^4] - E[\eta_2^4]\right|}{(H_s/4)^4}$$ (20)

In order to find the relationship between Err_κ and Err, in each case being simulated, the error of kurtosis can be estimated by using Eq.(19), and a data pair (Err, Err_κ) is obtained. Summarizing the cases where $Err \leq 0.1$, the error of kurtosis against the error of skewness is displayed in Figure 10, where the symbol 'x' denotes the cases for $U_r \leq U_{r0}$ and 'o' for $U_r > U_{r0}$, while the dash line indicates $Err_\kappa = Err$. It can be observed that if Err is small, Err_κ is small as well; when Err increases, Err_κ does not necessarily become larger. However, it is found that the estimated errors of kurtosis are all below the dash line, which implies that if the estimated error of skewness is less than 0.1, the corresponding error of kurtosis should be less than the error of skewness, i.e., $Err_\kappa \leq Err$. Therefore, it is understandable that Eqs.(18) can also be used to predict the maximum error of kurtosis by using the KdV model.
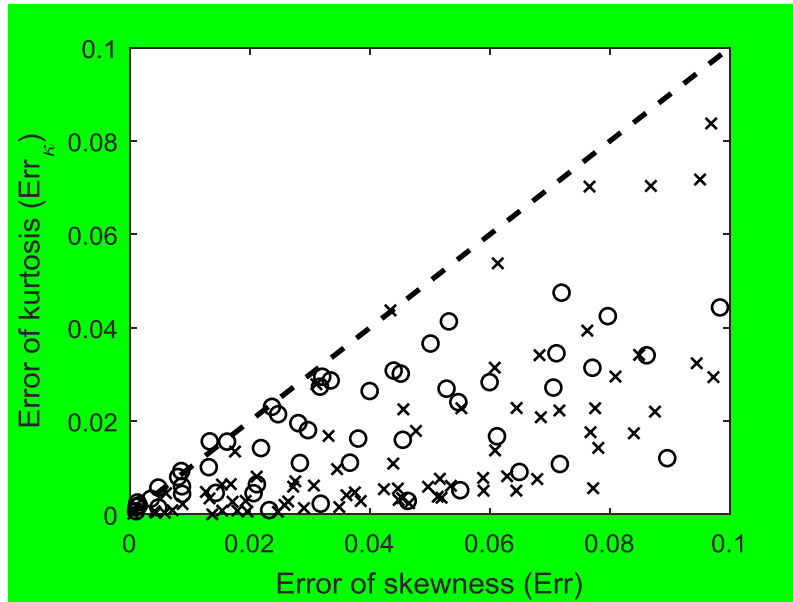
4.2 Justification of the KdV model's suitability

In order to model random waves in shallow water efficiently and accurately, one may employ a tool which can automatically determine whether to select the KdV model or not. For this purpose, Eqs. (18) can be reformulated and serve as such a criterion.

To do so, the user should specify a tolerance (Tol), such as 0.05 by looking at Figure 9, and allow the KdV model to be used when the condition $Err_i \leq Tol$ is met. With this, Eqs. (18) may be replaced by an expression in terms of the dimensionless significant wave height, i.e.,

$$H_{s1} = -0.127^{-1}(Tol + 3.985)(U_{rMin} - 7.092)^{-1} - 0.55U_{rMin} - 4.432 \tag{21a}$$

$$H_{s2} = -0.386^{-1}(Tol + 0.15)(U_{rMax} + 1.24)^{-1} + 0.146U_{rMax} + 0.209 \tag{21b}$$

where U_{rMin} and U_{rMax} are the minimum and maximum Ursell number respectively for the KdV model to be employed. Based on Eqs.(21), the graphs of $H_{s1} \sim U_{rMin}$ and $H_{s2} \sim U_{rMax}$ with respect to $Tol = 0.05$ is shown in Figure 11, which illustrates the regions in which a suitable model should be employed.
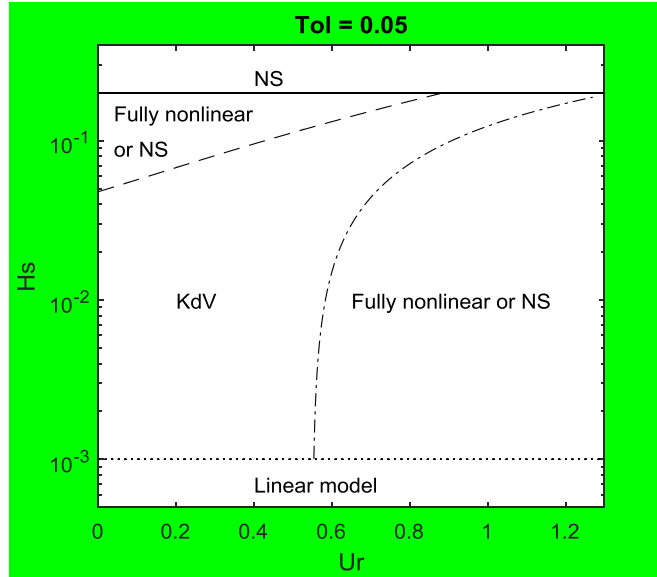

Figure 11. Suitability of the KdV equation.

$H_{s1} \sim U_{rMin}$: '- - -', $H_{s2} \sim U_{rMax}$: '- · -', $H_s = 0.001$: '····', $H_s = 0.2$: '——'

Based on these aforementioned, it is suggested that the following conditions

$$0.001 \leq H_s \leq 0.2 \tag{22a}$$

$$Max\{0, U_{rMin}\} \leq U_r \leq U_{rMax} \tag{22b}$$

as the criterion for selecting the KdV equation for modelling the unidirectional (two-dimensional) random waves in shallow water on large-spatial and long-temporal scale. That is to say, if the conditions of Eqs.(22) are met, the KdV equation is sufficient. Otherwise, linear or fully nonlinear model should be employed, depending on the magnitude of the dimensionless significant wave height. It is noted that for very strong nonlinear cases wave breaking will occur, so that potential models will not be suitable and NS model should be employed.

5   Conclusion

The main contribution of this paper is to give a group of formulas for estimating the error in terms of skewness when the KdV equation is employed to simulate nonlinear random shallow water waves on a large scale for a long duration in a phase resolved manner. The suggested formulas can give good predictions on the errors of the statistics by using the KdV model as long as the errors are less than 10% within the range $0.001 \leq H_s \leq 0.2$ and $0.01 \leq U_r \leq 10$, where the ranges of wave steepness and Ursell number are considered to cover the most cases in practice.

Based on the formulas, the suitable region for the KdV model is presented in terms of wave steepness and Ursell number. For a fixed wave steepness, the KdV model can only be employed in a certain range of Ursell number determined by that steepness and user specified tolerance, which is quite different from the qualitative indication available in literature.

The contribution of this study is twofold, e.g., it shows how reliable are the results obtained by using the KdV model after running the code, and whether it should be employed in order to obtain acceptable results before running any code. However, it should be pointed out that the formulas given in this paper are based on the cases of unidirectional waves, whereas for spreading seas, the Boussinesq equation should be adopted and will be studied in the future. Furthermore, the wind input and dissipation due to wave breaking are important factors for wave propagation on large spatiotemporal scale to achieve the equilibrium. However, the effects of wind input can be neglected, and the conclusion of this paper may still hold for waves featuring narrow spectrum, provided the wave age is not too small [74]. Additionally, as pointed out in this study, the KdV model is considered unsuitable in cases involving wave breaking, while dissipation due to breaking is insignificant in nonbreaking cases. Nevertheless, to

investigate the suitability of the KdV model before achieving the equilibrium, simulations of transient waves on local scale are required, which will be studied systematically in the future.

Appendix

The formulations for each part of the vertical velocity are given as

$$V_1 = F^{-1}\left\{K tanh(Kh) F\{\tilde{\phi}\}\right\} \tag{A. 1}$$

$$V_2 = F^{-1}\left\{-K tanh(Kh) F\{\eta V_1\} - i\boldsymbol{K} \cdot F\{\eta \nabla \tilde{\phi}\}\right\} \tag{A. 2}$$

$$V_3 = F^{-1}\left\{KC_h\left[F\{V_{3,s} + V_{3,b}\}\right]\right\} \tag{A. 3}$$

$$V_4 = F^{-1}\left\{KC_h\left[e_h F\{\eta(V - V_1)\} + F\left\{\eta F^{-1}\{e_h F\{V - V_1\}\}\right\} + F\{V_{4,s} + V_{4,b}\}\right]\right\} \tag{A. 4}$$

where $e_h = e^{-2Kh}$, $C_h = (1 + e_h)^{-1}$, and

$$V_{3,s} = \frac{1}{2\pi}\int \tilde{\phi}'\left[1 - (1 + D^2)^{-3/2}\right]\nabla' \cdot \left[(\eta' - \eta)\nabla'R^{-1}\right] d\boldsymbol{X}' \tag{A. 5}$$

$$V_{4,s} = \frac{1}{2\pi}\int V'R^{-1}\left[1 - (1 + D^2)^{-1/2}\right]d\boldsymbol{X}' \tag{A. 6}$$

$$V_{3,b} = -\frac{1}{2\pi}\int 12h^2(\eta' + \eta)R_B^{-5}\tilde{\phi}' d\boldsymbol{X}' + \frac{1}{2\pi}\int \tilde{\phi}'[\boldsymbol{R} \cdot \nabla'\eta' - (\eta' + \eta) - 2h] \cdot (r_B^{-3} - R_B^{-3}) d\boldsymbol{X}' \tag{A. 7}$$

$$V_{4,b} = \frac{1}{2\pi}\int V'[R_B^{-1} - 2h(\eta' + \eta)R_B^{-3} - r_B^{-1}]d\boldsymbol{X}' \tag{A. 8}$$

with $r_B = \sqrt{R^2 + (\eta' + \eta + 2h)^2}$, $R = |\boldsymbol{R}| = |\boldsymbol{X}' - \boldsymbol{X}|$, $D = (\eta' - \eta)/R$, $D_B = (\eta' + \eta)/R_B$, $R_B = \sqrt{R^2 + 4h^2}$ and the variables with the prime indicate those at source point $(\boldsymbol{X}', Z')$. Note that $V_{3,s}$ and $V_{4,s}$ are the surface integral parts and $V_{3,b}$ and $V_{4,b}$ are the bottom integral parts. In deep water situations, the latter is not involved, and Fructus, et al. [22] has rewritten $V_{4,s}$ and transformed the dominant part into the third order convolutions, i.e.,

$$F\{V_{4,s}\} = -\frac{K}{2}\left[KF\{\eta^2 V\} - 2F\left\{\eta F^{-1}\{KF\{\eta V\}\}\right\} + F\left\{\eta^2 F^{-1}\{KF\{V\}\}\right\}\right]$$

$$+ \frac{K}{2\pi}F\left\{\int \frac{V'}{R}\left(1 - \frac{1}{\sqrt{1 + D^2}} - \frac{1}{2}D^2\right)d\boldsymbol{X}'\right\} \tag{A. 9}$$

The rest formulations are omitted for simplicity which can be found in Fructus, et al. [22].

References

[1] W. Xiao, Study of directional ocean wavefield evolution and rogue wave occurrence using large-scale phase-resolved nonlinear simulations (PhD thesis), Cambridge, United States: Massachusetts Institute of Technology, 2013.

[2] K. Hasselmann, "On the nonlinear energy transfer in a gravity wave spectrum. Part 1: General theory," *J. Fluid Mech.,* vol. 12, p. J. Fluid Mech., 1962.

[3] O. M. Phillips, "Wave interactions - the evolution of an idea," *Journal of Fluid Mechanics,* vol. 106, pp. 215-227, 1981.

[4] G. J. Komen, L. Cavaleri, M. Donelan, K. Hasselmann, S. Hasselmann and P. A. Janssen, Dynamics and modeling of ocean waves, New York: Cambridge University Press, 1996.

[5] I. Lavrenov, Wind-waves in oceans: dynamics and numerical simulations, Berlin Heidelberg: Springer Science & Business Media, 2003.

[6] L. Cavaleri, J. Alves, F. Ardhuin, A. Babanin, M. Banner, K. Belibassakis, M. Benoit, M. Donelan, J. Groeneweg, T. H. C. Herbers, P. Hwang, P. A. E. M. Janssen, T. Janssen, I. V. Lavrenov, R. Magne, J. Monbaliu, M. Onorato, V. Polnikov, D. Resio, W. E. Togers, A. Sheremet, J. McKee Smith, H. L. Tolman, G. v. Vledder, J. Wolf and I. Young, "Wave modelling - The state of the art," *Progress in Oceanography,* vol. 75, pp. 603-674, 2007.

[7] A. Sheremet, J. R. Davis, M. Tian, J. L. Hanson and K. K. Hathaway, "TRIADS: a phase-resolving model for nonlinear shoaling of directional wave spectra," *Ocean Modelling,* vol. 99, p. 60–74, 2016.

[8] M. S. Longuet-Higgins and E. D. Cokelet, "The deformation of steep surface waves on water. I. A numerical method of computation," *Pro. R. Soc. Lond. A,* vol. 350, pp. 1-26, 1976.

[9] S. T. Grilli, P. Guyenne and F. Dias, "A fully non-linear model for three-dimensional overturning waves over an arbitrary bottom," *International Journal for Numerical Methods in Fluids,* vol. 35, pp. 829-867, 2001.

[10] G. X. Wu and R. Eatock-Taylor, "Finite element analysis of two dimensional non-linear transient water waves," *Appl. Ocean Res.,* vol. 16, pp. 363-372, 1994.

[11] Q. W. Ma, Numerical simulation of nonliear interaction between structures and steep waves (PhD Thesis), London: Department of Mechanical Enginieering, University College London, UK, 1998.

[12] Q. W. Ma and S. Yan, "Quasi ALE finite element method for nonlinear water waves," *Journal of Computational Physics,* vol. 212, pp. 52-72, 2006.

[13] S. Yan, Numerical simulation on nonlinear response of moored floating structures to steep waves (PhD thesis), London, UK: School of Engineering and Mathematical Sciences, City University London, 2006.

[14] T. E. Baldock and C. Swan, "Numerical calculations of large transient water waves," *Applied Ocean Research,* vol. 16, no. 2, pp. 101-112, 1994.

[15] T. B. Johannessen and C. Swan, "Nonlinear transient water waves—part I. A numerical method of computation with comparisons to 2-D laboratory data," *Applied Ocean Research,* vol. 19, no. 5, pp. 293-308, 1997.

[16] D. Chalikov and A. V. Babanin, "Three-Dimensional Periodic Fully Nonlinear Potential Waves," in *ASME 2013 32nd International Conference on Ocean, Offshore and Arctic Engineering*, Nantes, France, 2013.

[17] J. W. Kim and R. C. Ertekin, "A numerical study of nonlinear wave interaction in regular and irregular seas: irrotational Green–Naghdi model," *Marine structures,* vol. 13, no. 4, pp. 331-347, 2000.

[18] B. West, K. Brueckner, R. Janda, D. Milder and R. Milton, "A new numerical method for surface hydrodynamics," *Journal of Geophysical Research: Oceans,* vol. 92, no. C11, pp. 11803-11824, 1987.

[19] D. G. Dommermuth and D. K. P. Yue, "A high-order spectral method for the study of nonlinear gravity waves," *J. Fluid Mech.,* vol. 184, pp. 267-288, 1987.

[20] D. P. Nicholls, "Traveling Water Waves: Spectral Continuation Methods with Parallel Implementation," *Journal of Computational Physics,* vol. 143, no. 1, pp. 224-240, 1998.

[21] D. Clamond and J. Grue, "A fast method for fully nonlinear water-wave computations," *J. Fluid Mech.,* vol. 447, pp. 337-355, 2001.

[22] D. Fructus, D. Clamond, J. Grue and O. Kristiansen, "An efficient model for three-dimensional surface wave simulations Part I: Free space problems," *Journal of Computational Physics,* vol. 205, pp. 665-685, 2005.

[23] J. Grue, "On four highly nonlinear phenomena in wave theory and marine dydrodynamics," *Applied Ocean Research,* vol. 24, pp. 261-274, 2002.

[24] J. Grue, "Computation formulas by FFT of the nonlinear orbital velocity in three-dimensional surface wave fields," *J. Eng. Math.,* vol. 67, pp. 55-69, 2010.

[25] J. Wang and Q. W. Ma, "Numerical techniques on improving computational efficiency of Spectral Boundary Integral Method," *International Journal for Numerical Methods in Engineering,* vol. 102, no. 10, pp. 1638-1669, 2015a.

[26] G. Ducrozet, E. Bonnefoy, D. L. Touze and P. Ferrant, "3-D HOS simulation of extreme waves in open seas," *Nat. Hazards Earth Syst. Sci.,* vol. 7, pp. 109-122, 2007.

[27] D. Kriebel, "Nonlinear wave interaction with a vertical circular cylinder. Part I: Diffraction theory," *Ocean Engineering,* vol. 17, no. 4, pp. 345-377, 1990.

[28] D. Kriebel, "Nonlinear wave interaction with a vertical circular cylinder. Part II: Wave run-up," *Ocean Engineering,* vol. 19, no. 1, pp. 75-99, 1992.

[29] V. E. Zakharov, "Stability of periodic waves of finite amplitude on the surface of a deep fluid," *Sov. Phys. J. Appl. Mech. Tech. Phys,* vol. 9, pp. 86-94, 1968.

[30] S. Y. Annenkov and V. I. Shrira, "Numerical modelling of water-wave evolution based on the Zakharov equation," *Journal of Fluid Mechanics,* vol. 449, pp. 341-371, 2001.

[31] V. E. Zakharov, A. I. Dyachenko and O. A. Vasilyev, "New method for numerical simulation of a nonstationary potential flow of incompressible fluid with a free surface," *European Journal of Mechanics-B/Fluids,* vol. 21, no. 3, pp. 283-291, 2002.

[32] D. J. Benney and G. J. Roskes, "Wave instabilities," *Studies in Applied Mathematics,* vol. 48, pp. 377-385, 1969.

[33] A. Davey and K. Stewartson, "On three-dimensional packets of surface waves," *Proc. R. Soc. Lond. A,* vol. 388, pp. 101-110, 1974.

[34] C. Mei, The applied dynamics of ocean surface waves, New York: Wiley, 1983.

[35] D. J. Korteweg and G. de Vries, "On the change of form of long waves advancing in a rectangular cannal, and on a new type of long stationary waves," *Phil. Mag.,* vol. 39, pp. 422-443, 1895.

[36] T. B. Benjamin, J. L. Bona and J. J. Mahony, "Model equations for long waves in nonlinear dispersive systems," *Philosophical Transactions of the Royal Society of London A: Mathematical, Physical and Engineering Sciences,* vol. 272, no. 1220, pp. 47-78, 1972.

[37] B. B. Kadomtsev and V. I. Petviashvili, "On the stability of solitary waves in weakly dispersive media," *Soviet Physics,* vol. 15, pp. 539-541, 1970.

[38] J. T. Kirby and P. Vengayil, "Nonresonant and resonant reflection of long waves in varying channels," *Journal of Geophysical Research,* vol. 93, no. C9, pp. 10782-10796, 1988.

[39] T. Kakutani, "Effect of an Uneven Bottom on Gravity Waves," *J. Phy. Soc. Japan,* vol. 30, pp. 272-276, 1971.

[40] J. W. Miles, "Wave evolution over a gradual slope with turbulent friction," *Journal of Fluid Mechanics,* vol. 133, pp. 207-216, 1983.

[41] G. A. EI, R. H. J. Grimshaw and A. M. Kamchatnov, "Evolution of solitary waves and undular bores in shallow-water flows over a gradual slope with bottom friction," *Journal of Fluid Mechanics,* vol. 585, pp. 213-244, 2007.

[42] G. Wei and J. T. Kirby, "Time-dependent numerical code for extended Boussinesq equations," *Journal of Waterway, Port, Coastal, and Ocean Engineering,* vol. 121, no. 5, pp. 251-261, 1995.

[43] G. Wei, J. T. Kirby, S. T. Grilli and R. Subramanya, "A fully nonlinear Boussinesq model for suface waves. Part 1. Highly nonlinear unsteady waves," *J. Fluid Mech.,* vol. 294, pp. 71-92, 1995.

[44] P. A. Madsen, H. B. Bingham and H. Liu, "A new Boussinesq method for fully nonlinear waves from shallow to deep water," *Journal of Fluid Mechanics,* vol. 462, pp. 1-30, 2002.

[45] P. J. Lynett and P. L. F. Liu, "Linear analysis of the multi-layer model," *Coastal Engineering,* vol. 51, pp. 439-454, 2004.

[46] P. A. Madsen, O. R. Sørensen and H. A. Schäffer, "Surf zone dynamics simulated by a Boussinesq type model. Part II: Surf beat and swash oscillations for wave groups and irregular waves," *Coastal Engineering,* vol. 32, no. 4, pp. 289-319, 1997.

[47] G. Wei, J. T. Kirby and A. Sinha, "Generation of waves in Boussinesq models using a source function method," *Coastal Engineering,* vol. 36, pp. 271-299, 1999.

[48] Q. Chen, J. T. Kirby, R. A. Dalrymple, A. B. Kennedy and A. Chawla, "Boussinesq modeling of wave transformation, breaking, and runup. II: 2D," *Journal of Waterway, Port, Coastal, and Ocean Engineering,* vol. 126, no. 1, pp. 48-56, 2000.

[49] A. B. Kennedy, Q. Chen, J. T. Kirby and R. A. Dalrymple, "Boussinesq modeling of wave transformation, breaking, and runup. I: 1D," *Journal of Waterway, Port, Coastal, and Ocean Engineering,* vol. 126, no. 1, pp. 39-47, 2000.

[50] P. A. Madsen and D. R. Fuhrman, "High-Order Boussinesq-Type Modelling of Nonlinear Wave Phenomena in Deep and Shallow Water," in *Adcances in Numerical Simulation of Nonlinear Water Waves*, Singagpore, World Scienticif Publishing Co. Pte. Ltd., 2010, pp. 245-286.

[51] A. Kokorina and E. Pelinovsky, Evolution of unidirectional random waves in shallow water (the Korteweg-de Vries model), arXiv preprint nlin/0306044 ed., Ithaca, NY, US: Cornell University Library, 2003.

[52] E. Pelinovsky and A. Sergeeva, "Numerical modeling of the KdV random wave field," *European Journal of Mechanics B/Fluids,* vol. 25, pp. 425-434, 2006.

[53] A. Sergeeva, E. Pelinovsky and T. Talipova, "Nonlinear random wave field in shallow water: variable Korteweg-de Vries framework," *Natural Hazards and Earth System Science,* vol. 11, no. 2, pp. 323-330, 2011.

[54] D. Dutykh, M. Chhay and F. Fedele, "Geometric numerical schemes for the KdV equation," *Computational Mathematics and Mathematical Physics,* vol. 53, no. 2, pp. 221-236, 2013.

[55] A. Toffoli, M. Onorato, A. R. Osborne and J. Monbaliu, "Non-Gaussian properties of shallow water waves in crossing seas," in *Extreme ocean waves*, Springer International Publishing, 2016, pp. 75-91.

[56] J. Wang, Q. W. Ma and S. Yan, "Numerical Investigation on Spetrum Evolution of Random Waves in Shallow Water based on KdV and Fully Nonlinear Model," in *Proceedings of the ASME 2016 35th International Conference on Ocean, Offshore and Arctic Engineering*, Busan, Korea, 2016.

[57] J. Grue, E. N. Pelinovsky, D. Fructus, T. Talipova and C. Kharif, "Formation of undular bores and solitary waves in the Strait of Malacca caused by the 26 December 2004 Indian Ocean tsunami," *Journal of Geophysical Research: Oceans,* vol. 113, no. C5, pp. 1-14, 2008.

[58] P. A. E. M. Janssen, "On some consequences of the canonical transformation in the Hamiltonian theory of water waves," *Journal of Fluid Mechanics,* vol. 637, pp. 1-44, 2009.

[59] A. R. Osborne, M. Serio, L. Bergamasco and L. Cavaleri, "Solitons, cnoidal waves and nonlinear interactions in shallow-water ocean surface waves," *Phasica D,* vol. 123, pp. 64-81, 1998.

[60] V. Sriram, I. Didenkulova, S. Schimmels, A. Sergeeva and N. Goseberg, "Long wave propagation, shoaling and run-up in nearshore areas," *Coastal Engineering Proceedings,* vol. 1, no. 34, p. 20, 2014.

[61] V. Sriram, I. Didenkulova, A. Sergeeva and S. Schimmels, "Tsunami evolution and run-up in a large scale experimental facility," *Coastal Engineering,* vol. 11, pp. 1-12, 2016.

[62] C. Kharif, E. Pelinovsky and A. Slunyaev, Rogue Waves in the Ocean, Berlin Heidelberg: Springer-Verlag, 2009.

[63] E. Lo and C. C. Mei, "A numerical study of water-wave modulation based on a higher-order nonlinear Schrödinger equation," *J. Fluid Mech.,* vol. 150, pp. 395-416, 1985.

[64] D. Clamond, D. Fructus, J. Grue and O. Kristiansen, "An efficient model for three-dimensional surface wave simulations. Part II: Generation and absorption," *Journal of Computational Physics,* vol. 205, pp. 686-705, 2005.

[65] F. Shi, J. T. Kirby, J. C. Harris, J. D. Geiman and S. T. Grilli, "A high-order adaptive time-stepping TVD solver for Boussinesq modeling of breaking waves and coastal inundation," *Ocean Modelling,* vol. 43, pp. 36-51, 2012.

[66] Y. Goda, "A comparative review on the functional forms of directional wave spectrum," *Coastal Engineering Journal,* vol. 41, no. 1, pp. 1-20, 1999.

[67] J. Wang and Q. W. Ma, "Numerical Investigation on Limitation of Boussinesq Equation for Generating Focusing Waves," *Procedia Engineering,* vol. 126, pp. 597-601, 2015b.

[68] C. H. Kim, Nonlinear Waves and Offshore Structure, Singapore: World Scientific Publishing Co. Pte. Ltd, 2008.

[69] M. Tucker, P. Challenor and D. Carter, "Numerical simulation of a random sea: a common error and its effect upon wave group statistics," *Applied ocean research,* vol. 6, no. 2, pp. 118-122, 1984.

[70] S. Elgar, R. T. Guza and R. J. Seymour, "Wave group statistics from numerical simulations of a random sea," *Applied ocean research,* vol. 7, no. 2, pp. 93-96, 1985.

[71] D. Fructus, C. Kharif, M. Francius, Ø. Kristiansen, D. Clamond and J. Grue, "Dynamics of crescent water wave patterns," *Journal of Fluid Mechanics,* vol. 537, pp. 155-186, 2005.

[72] F. Ursell, "The long wave paradox in the theory of gravity waves," *Proc. Camb. Phil. Soc,* vol. 49, pp. 685-694, 1953.

[73] M. Onorato and P. Suret, "Twenty years of progresses in oceanic rogue waves: the role played by weakly nonlinear models," *Natural Hazards,* pp. 1-8, 2016.

[74] K. B. Dysthe, K. Trulsen, H. E. Krogstad and H. Socquet-Juglard, "Evolution of a narrow-band spectrum of random surface gravity waves," *Journal of Fluid Mechanics*, vol. 478, pp. 1-10, 2003.